Photonic Crystal Nanobeam Cavities for Tunable Filter and Router Applications

Parag B. Deotare, *Student Member, IEEE*, Leonard C. Kogos, Irfan Bulu, and Marko Lončar, *Senior Member, IEEE*

(Invited Paper)

***Abstract*—We investigate the suitability of photonic crystal nanobeam cavities for interconnect applications. Owing to their small footprint, exactly the same as that of an optical waveguide, as well as ultrahigh quality factor resonances that they support, nanobeam cavities are attractive candidates for realization of densely integrated on-chip optical networks. We discus tunability of these filters using thermo-optic, electromechanic, and optomechanic effects, and we compare different reconfiguration strategies in terms of tuning hold power, tuning efficiency, and maximum operating frequency.**

***Index Terms*—Photonic crystal, tunable filters.**

I. Introduction

DURING the last century we have witnessed an exponential growth in optical communications, driven by society's demand for more information. The idea of using photons instead of electrons as long-distance information carriers became a reality, and was enabled by important technological breakthroughs including the invention of optical fibers and lasers. In fact, today long distance communication is dominated by optical fibers, the best information channel known to man, which allow information to be efficiently transferred at rates higher than 40 Gb/s. On the other hand, short distance communication (e.g., on-chip, between different parts of microprocessor) is still dominated by electrons and information is transferred using electric wires. Losses in these electronic interconnects account for more than $50\,\%$ of the consumed energy causing excessive heating [1]. As technology strives to achieve higher device densities, issues related to poor heat dissipation capabilities [2] and delays [3] become prominent. For the past decade, researchers have been looking into optical interconnects as an efficient alternative for electrical interconnects to solve the last mile problem [4]–[6]. Optical interconnects not only reduce ohmic losses but also allow for a large operation bandwidth and can take advantage of wavelength division multiplexing (WDM) technique to transfer information at an extremely high rate at very low power [5].

Short distance communication can be divided into two parts: 1) between two processing units (for example, in a computing cluster); and 2) between multiple cores of a processor (on chip). Enormous effort has been put in to cost effectively implement the matured technology used for long distance communication to solve the former issue [7] (for example, fiber to the home technology [8]). However, the latter demands new breakthroughs in technology due to its on-chip requirements [9], [10], and new areas of research emerged as industry and researchers explored various ways to manipulate light on chip. These on-chip optical interconnects require integrable passive and active optical components like light sources, waveguides, amplifiers, filters, modulators, routers, switches, etc. In this study, we focus on an optical filter, which if reconfigured can be used as a switch or a router.

An optical filter removes certain wavelengths in the spectrum of an incoming optical signal by leveraging losses in the system (e.g., material absorption, scattering, etc.), interference of light, or combination of both effects. For example, filtering effects in the case of stained (colored) glass is material absorption, while in the case of thin films (e.g., oil on water) is interference. On-chip version of an interference filter is unbalanced Mach–Zehnder interferometer [11] that removes all wavelengths that satisfy $2 \cdot n_{\mathrm{eff}} \cdot \Delta L = (2 \cdot m + 1) \cdot \lambda$, where ΔL is the path length difference, n_{eff} is the effective index, and λ is the operating wavelength. The idea of interference can be further extended to optical resonators to form extremely narrow optical filters. For example, waveguide coupled to one [12] or many [13], [14] ring resonators can be used to filter-out wavelengths that satisfy the resonant condition of the resonator (or an array of the resonators). This approach takes advantage of intrinsic resonator losses (typically bending losses) to achieve filtering function. Another common resonator platform that has been used for filtering purpose (as well high-resolution spectroscopy) is a Fabry–Perót cavity, formed by two highly reflective mirrors. In contrast to traveling-wave ring-resonators aforementioned, Fabry–Perót cavity transmits wavelengths that satisfy resonant condition—the mechanism that is often referred to as resonant tunneling—and reject the rest. In this study, we focus on high quality factor (Q) on-chip Fabry–Perót type optical resonators, photonic crystal nanobeam cavity (PCNC) that

Manuscript received July 13, 2012; revised September 10, 2012; accepted September 29, 2012. Date of publication October 22, 2012; date of current version April 3, 2013. This work was supported in part by the National Science Foundation (NSF) through the NSF Career Award, in part by a gift from Schlumberger-Doll Research Center (Cambridge, MA), in part by the Massachusetts Institute of Technology and in part by the Harvard School of Engineering and Applied Sciences.

P. B. Deotare is with the Organic and Nanostructured Electronics Laboratory, Massachusetts Institute of Technology, Cambridge, MA 02139 USA (e-mail: pdeotare@mit.edu).

L. C. Kogos is with the Schlumberger Doll-Research Center, Cambridge, MA 02139 USA (e-mail: leokogos@gmail.com).

I. Bulu and M. Lončar are with the Harvard School of Engineering and Applied Sciences, Cambridge MA 02138 USA (e-mail: irfan@seas.harvard.edu; oncar@seas.harvard.edu).

Color versions of one or more of the figures in this paper are available online at http://ieeexplore.ieee.org.

Digital Object Identifier 10.1109/JSTQE.2012.2225828

take advantage of photonic bandgap engineering to realize high-reflectivity mirrors. Q is a dimensionless quantity used to characterize a resonator's full-width half-maximum bandwidth, and it relates the rate of energy loss of the resonator: a high Q resonator stores energy for longer period of time and has a smaller bandwidth compared to a low Q resonator. This makes high Q resonators excellent candidates for realization of optical filters with sharp resonances. However, the rate at which resonator can be "charged" with and "depleted" of photons, and thus the speed at which information can be transmitted through the resonator is inversely proportional to the Q of the resonator: $1/\tau_{\text{photon}} = \omega/Q$, where τ_{photon} is a photon lifetime of the resonator, and $\omega = 2 \cdot \pi \cdot c/\lambda$, and c is the speed of light. As a rule of thumb, cavity with $Q \approx 10^6$ has $\tau_{\text{photon}} \approx 1$ ns for telecom wavelength range, which limits operation speed to below 1 GHz. Therefore, tradeoff between the resonator linewdith and speed of operation needs to be considered.

Compared to electronic devices, microfabricated photonic devices are far more sensitive to fabrication tolerances. Therefore, the ability to perform postfabrication wavelength trimming, as well as dynamical tuning/ reconfiguration, is an important feature for integrated photonics. Reconfiguration of optical devices can be achieved by changing its effective optical length either by changing the effective index of the optical modes or the physical length of the devices (e.g., stretching). The former techniques can be classified into two types: 1) direct, that cause change in refractive index due to internal perturbations, and 2) indirect, that cause change in the effective refractive index of mode by controlling its overlap with the structure. Reconfiguration methods based on thermo-optic effect [15]–[17] and free carrier injection [18] fall under direct type while those using electromechanical and optomechanical [19]–[21] effects are categorized under indirect methods. We first review the direct tuning techniques for PCNC, that take advantage of thermo-optic effect. Next, by leveraging mechanical degrees of freedom of free-standing PCNCs we introduce electromechanical and optomechanical reconfiguration techniques based on electrical and optical forces, respectively. Electromechanical reconfiguration is extremely efficient since it requires zero hold power (the power to hold the device in a reconfigured state), but in turn requires introduction of electrical contacts to our devices which increases the footprint of the devices. On the other hand, an optomechanical reconfiguration method does not suffer from increased footprint and is an all-optical approach, but does require steady-state hold power. We note that both techniques have negligible effect on the Q of the devices.

II. Photonic Crystal Nanobeam Cavities

The characterization schematic, SEM micrograph of the fabricated structure, mode profile, and experimental transmission of PCNC cavity are shown in Fig. 1. The devices were tested via transmission measurements using a butt-coupling technique [see Fig. 1(a)]. Briefly, light was coupled using tapered lensed fiber (Oz optics, NA 0.4) into the SU-8 waveguide. An inverse taper geometry (taper length of 200 μm and a taper tip width of 50 nm) was used as a mode-size converter to efficiently couple

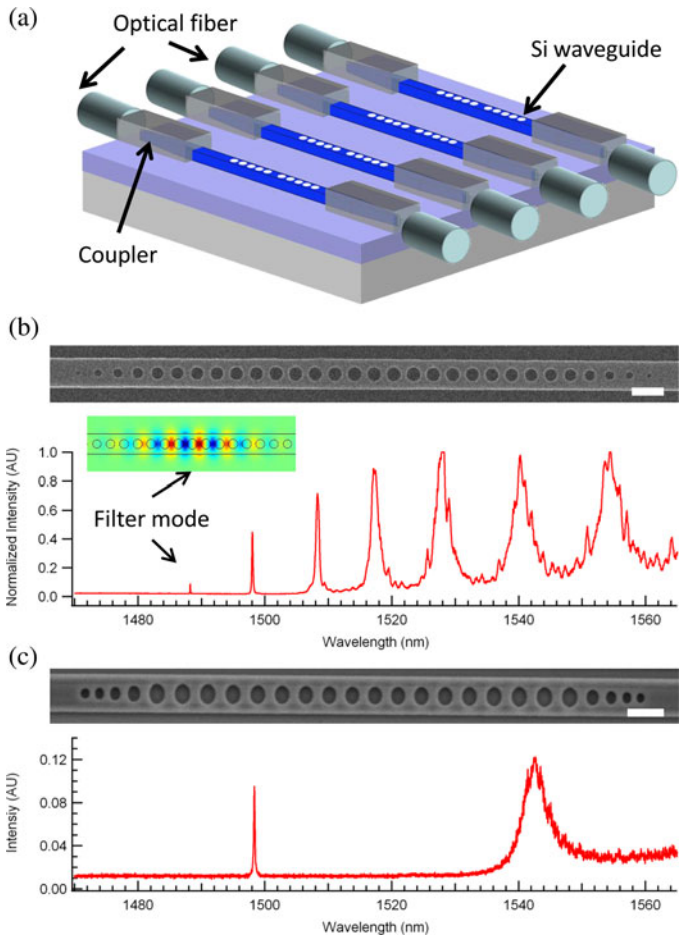

Fig. 1. PCNC. (a) Schematic showing a butt coupling technique using spot-size converter couplers based on polymer waveguides and inverse-tapered silicon waveguides for transmission measurement of devices. (b) SEM image of the single PCNC (scalebar = 0.5 μm) designed using a deterministic approach along with transmission data. The inset shows the electric field mode profile of the fundamental resonance. (c) SEM image of the single PCNC (scalebar = 0.5 μm) designed using an iterative approach along with transmission data.

the light from SU-8 waveguides into the silicon waveguides [22] (waveguide width of 700 nm). This was necessary due to the mode size mismatch between the fiber and the silicon waveguide. SU-8 waveguides had significantly larger cross section dimensions ($3 \times 3\,\mu$m) when compared to silicon waveguides (700 nm $\times$ 220 nm) which allowed for an efficient coupling between the fiber mode and the SU-8 waveguide mode. At the output, a similar coupling method was used except that the light was collected with a SM tapered lensed fiber (SM tapered fibers have lower taper conversion loss). We estimated the coupling loss associated with the spot-size converters to be 2 ± 0.5 dB. The devices were characterized using tunable lasers (Agilent 81682, Santec TSL-510) and a sensitive InGaAs detector (EO systems, IGA $-$ 010 $-$ TE2 $-$ H).

The devices were fabricated in the technologically relevant silicon-on-insulator (SOI) platform consisting of a silicon device layer of 220 nm and a buried oxide layer of 2 μm. The patterns were written using a negative ebeam resist XR $-$ 1451 $-$ 002 with a 100 keV ebeam lithography tool. The patterns were then transferred to silicon using ICP-RIE etch, a C_4F_8 and SF_6

chemistry. SU-8 polymer coupling pads were then written on each end of the device to couple light in and out of chip. The sample was then cleaved through the SU-8 pads.

The cavity shown in Fig. 1(b) was designed using the deterministic approach outlined in our previous work [23], [24] that results in cavities that feature high transmission at the cavity resonance: $Q > 10^7$ with transmission of $97\,\%$ [24]. A typical transmission spectrum is shown in Fig. 1(b). The inset in Fig. 1(b) shows the electric field profile of the fundamental cavity resonance. The transmission data show zero transmission inside the bandgap of the photonic crystal except for the high Q cavity mode at 1490 nm which we refer to as our filter mode. The FSR of this filter is about 10 nm which may or may not be suitable for a filter application. For example, a larger FSR (communication window of an erbium amplifier is ~ 30 nm) is needed for applications in an optical add-drop multiplexer [25] and for on-chip spectroscopy applications [26], [27]. Large FSR, on the order of 40 nm can also be designed as shown in Fig. 1(c). These devices are designed using the approach described in [28]–[30] where the cavity is formed by using a multihole taper to improve mode matching to achieve ultrahigh Qs. The design also uses out coupling tapers to improve the transmission efficiency of the devices as seen in the SEM image in Fig. 1(c).

III. Reconfiguration Methods

A. Electrical Reconfiguration Methods

Thermo-optic coefficient, a measure of change in refractive index of a material with respect to temperature, of silicon is high and has a value $dn_{\mathrm{Si}}/dT = 1.86 \times 10^{-4}\ K^{-1}$. This feature can be utilized to tune the wavelength of Silicon-based PCNCs. For example, as little as $1\ K$ of temperature change is needed to change the resonant wavelength of the device by 100 pm.

Fig. 2(a) shows an optical image of the microheater fabricated over the PCNC and the cross section of the Ti heater section is shown in Fig. 2(b). The devices are embedded in oxide but can be designed to have ultrahigh $Q's$. To fabricate the device shown in Fig. 2(a), an additional plasma-enhanced chemical vapor deposition (PECVD) step was carried out after fabricating the SU-8 coupling pads, to deposit $1\,\mu$m of oxide followed by a photolithography step to define the heaters and electrodes. The oxide layer was needed to avoid any unwanted loss of light due to its interaction with the heaters. Titanium (100 nm) and gold (200 nm) were evaporated, followed by a lift off in Acetone. A second photolithography step was carried out to remove the gold above the heater region. This was necessary to achieve a highly resistive heating element that resulted in maximum voltage drop, and hence heating above the device. Finally, the sample was cleaved through the $SU8$ pads and the facets were polished to achieve optically flat surfaces. Fig. 2(c) shows the cross section of the simulated temperature profile of the device (for applied voltage of 0.2 V). The rectangles represent the heater (top) and the waveguide (bottom). As expected, the heaters are sufficiently close to heat the waveguides and at the same time, they are far enough to avoid any coupling with the optical field in the waveguide. The inset shows a section of the top view taken in the middle of the waveguide representing uniform heating. Thermal tuning of more than 7 nm was achieved for one device. The resistance of the heater was measured to be around $150\,\Omega$. Fig. 2(d) shows the detuning of the mode for various applied powers across the heater. Since electrical power is converted to heat, the detuning is linear with the applied power. Due to their simplicity, reconfigurable filters based on thermo-optic effects [31], [32] can prove to be useful for switching, filtering as well as postfabrication trimming applications. Direct thermo-optic effect-based reconfiguration scheme is relatively easy to implement but requires steady-state hold power to keep the system in reconfigured state.

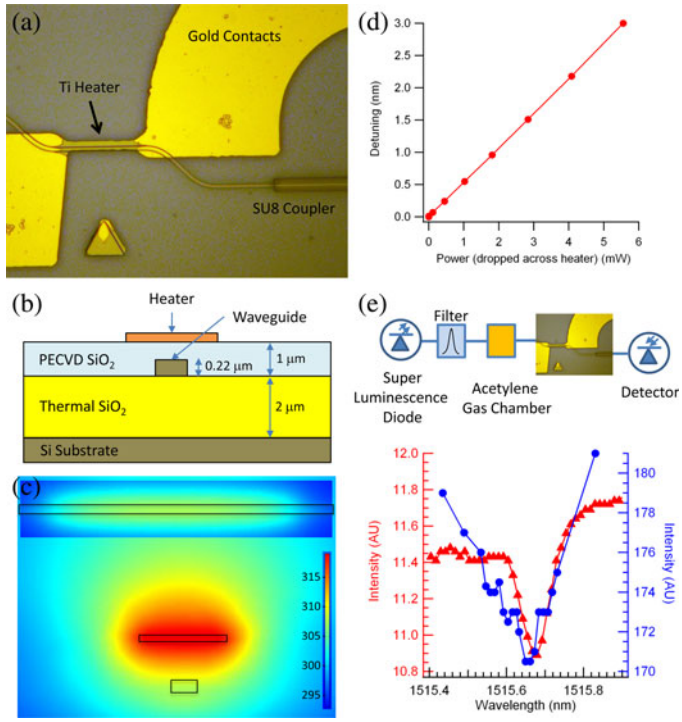

Fig. 2. Thermal reconfiguration of nanobeam cavities using microheaters. (a) Optical micrograph showing the device with microheaters. (b) Schematic of the cross section of the device (figure not to scale). (c) Cross section showing the simulated thermal profile of the structure (applied voltage of 0.2 V). The outlines of the heater (top) and the waveguide (bottom) are shown for guidelines. The inset shows a section of the top view taken in the middle of the waveguide. (d) Experimental results showing thermal detuning of the cavity mode for various dropped powers across the heater. (e) Schematic of the experimental setup used for measurement of absorption spectrum of Acetylene. The lower panel shows the results of the absorption spectrum line of acetylene obtained using a conventional bench top optical spectrum analyzer (filled red triangles) and the on-chip spectrometer (filled blue circles).

Fig. 2(e) outlines the application of the filter in spectroscopy. Light from a broadband super luminescence diode source was transmitted through an acetylene absorption chamber and the transmitted light was then coupled to a PCNC with a microheater. An optical filter was used to filter out the light transmitted outside the bandgap. The intensity of transmitted light was then measured while the cavity resonance was scanned by applying voltage to the microheater. Fig. 2(d) shows one absorption spectral line measured using a conventional bench-top grating spectrometer with a 0.1-nm resolution (red curve). The blue curve was obtained by thermally tuning the resonance of a PCNC (linewidth $= 0.12$ nm) across the spectral line. The

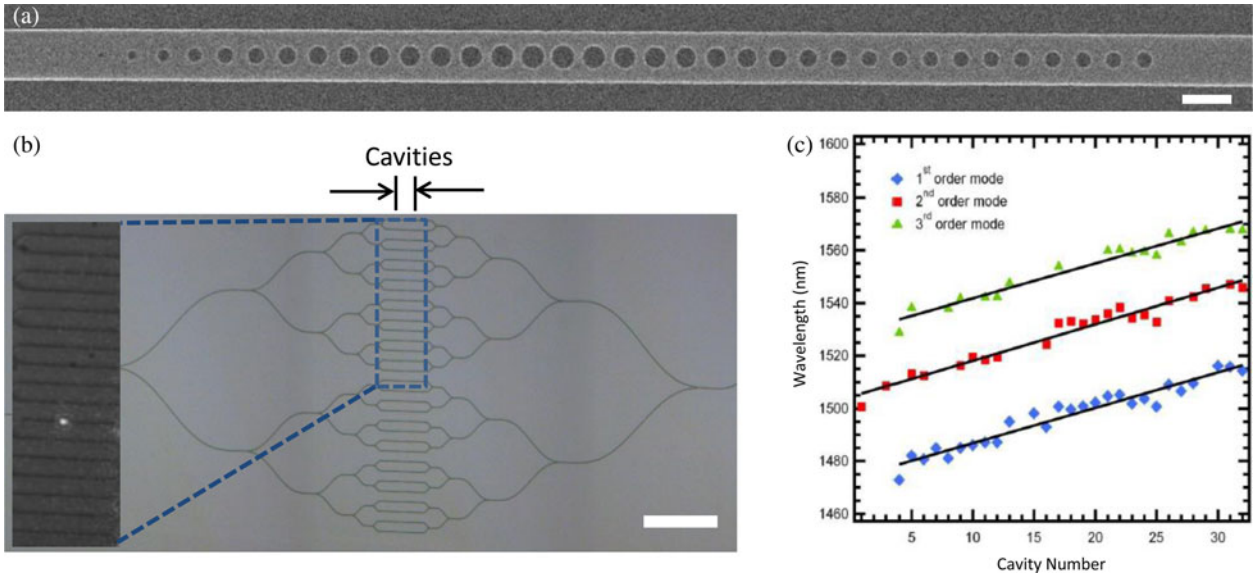

Fig. 3. On-chip spectrometer using nanobeam cavities. (a) SEM image of the single PCNC (scalebar $= 0.5\ \mu$m) designed using a deterministic approach. The devices were designed to scatter light in the vertical plane, by extending one of the Bragg mirrors (right side). (b) Optical micrograph showing 32 devices (scalebar $= 25\ \mu$m). Inset shows top view taken using an *IR* camera with only once cavity resonating at the input light wavelength. (c) Experimental data for the 32 devices showing the first three modes.

recovered spectra from the PCNC show a representative absorption dip. Discrepancies with spectra obtained using a bench-top spectrometer can be attributed to light leaking from higher order modes and slightly larger linewidth of the PCNC. This can be avoided by using devices with higher FSR and sharper resonances (smaller linewidth of filter mode).

By integrating number of PCNCs on the same cavity (see Fig. 3), a compact, fully integrated, on-chip spectrometer can be realized [27]. In general, resolution of a spectrometer based on dispersive component scales with size as higher resolutions require a longer optical path. The realization of a microspectrometer relies on the successful replacement of the dispersive element with a microcomponent. Significant progress has been made in integrated microspectrometers based on arrayed-waveguide gratings [33], [34], superprism-based spectrometers [35], grating spectrometers [36], [37], echelle grating spectrometer [38], and a diffractive grating spectrometer combined with thermo-optically tuned microring resonators [26]. All the nonmicroresonator techniques require larger foot print area since they are based on dispersion and suffer from large channel spacing due to low resolution. The microring/microdonut-based spectrometer has high resolution but require additional optical structures to scatter the light [27] for out of plane detection. A spectrometer based on PCNCs, can not only have high resolution but can also be designed to scatter light to an out-of-plane detector or used with integrated waveguide detectors [39]. For example, an array of III–V detectors can be easily integrated directly on top of the devices thus enabling the realization of a compact system. Here, we show a compact, robust, high resolution on-chip spectrometer based on an array of PCNCs tuned to operate at slightly different wavelengths. Since each device resonates at one particular wavelength, the spectrum of the incoming light can be reconstructed by detecting signal from the individual devices. The spectrometer consists of 32 PCNCs, with resonances 1 nm apart. The measured linewidth of each cavity was 120 pm which is on par with the resolutions obtained using a grating spectrometer. The cavities were designed to scatter light in the vertical plane, by extending one of the Bragg mirrors [see Fig. 3(a)]. This allowed us to view the scattered light using a sensitive IR camera [40]. An optical micrograph of the fabricated structure is shown in Fig. 3(b). The incoming light (from right) is split using multiple Y splitters and coupled into individual cavities. Inset shows an IR image of the cavity section with monochromatic input light from a laser. As expected, scattering of light is observed only from one cavity. Fig. 3(c) plots the first three modes for each of the cavities. The solid line shown the expected wavelengths for each of the modes. Results show an excellent agreement with theoretical values. The slight discrepancy from the solid line was attributed to the fabrication tolerances. This can be corrected using the thermal tuning scheme that we discussed previously, by fabricating individual microheaters above each device. This will not only allow for correcting fabrication errors but also minimize the number of devices required to cover a broad spectrum.

In addition to direct tuning methods discussed so far, indirect reconfiguration schemes based on mechanical deformation can also be implemented with the PCNC due to the flexibility of the structure. However, this requires the use of suspended devices in close proximity to a material which could induce perturbation to the effective refractive index. One way to achieve this would be to deform the devices toward the substrate [41] or toward another nanobeam. Another elegant method would be to use two PCNC's side by side such that the modes are coupled. From the physics of coupled harmonic oscillators, coupling generates modes which are symmetric and antisymmetric superpositions of the single cavity basis states [42], [43]. The frequency splitting between the modes is dependent on the strength of the coupling, which in this case is determined by the size of the

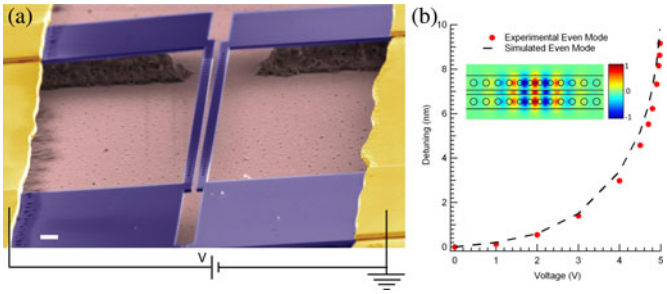

Fig. 4. Reconfigurable electromechanical optical filter (a) SEM image of a representative fabricated structure. The suspended silicon is in contact with gold electrodes seen at the edge of the image and is supported by islands of SiO_2 (scalebar $= 1\ \mu$m). (b) Experimental data showing the measured resonance for even supermode. The inset shows the electric field profile of the even mode.

gap (d). For small d, there is a strong coupling between the cavities. This leads to a large wavelength splitting between the modes, with the even mode (antisymmetric electric field profile) at longer wavelength, which is typical of coupled resonators. The wavelength of the odd mode (symmetric electric field profile) changes little with d, whereas the even mode disperses rapidly to longer wavelengths as d decreases. This asymmetry is indicative of the presence of second-order cross- and self-coupling effects between the coupled resonators in addition to the first-order effects of the index perturbation [42], [44]. As d shrinks below 100 nm, the field intensity of the gap antinode grows and becomes the dominant feature in the mode. These factors imply that the even mode would be a sensitive probe of the interbeam distance, and thus useful for reconfiguration applications.

The change in the optical frequency (wavelength) due to mechanical displacement can be obtained from the perturbation theory [45]. Detuning ($\Delta\omega$) due to optomechanics can be expressed in terms of the displacement field as

$$\Delta\omega = -\frac{\omega_0}{2}\frac{\langle E|\frac{d\epsilon}{dl}|E\rangle}{\langle E|\epsilon|E\rangle}\Delta l$$

$$\left\langle E\left|\frac{d\epsilon}{dl}\right|E\right\rangle = \int dA\frac{d\sigma}{dl}[\Delta\epsilon|E_{\|}|^2 - \Delta(1/\epsilon)|D_{\perp}|^2] \quad (1)$$

where $E_{\|}$ and $D_{\perp}$ are the parallel and normal components of electric field and the electric displacement field, $\Delta\epsilon$ is the dielectric perturbation, l is a parameter characterizing the displacement, i.e., change in the gap distance, and σ is the displacement field.

We take advantage of the mechanical flexibility of coupled PCNCs to realize reconfigurable devices that can be electrically actuated [46]–[48]. By applying a potential difference directly across the nanobeams, an attractive electrostatic force can be induced between the two nanobeams, resulting in a decrease of the gap between the nanobeam [see Fig. 4(a)]. This, in turn, results in a change of the resonant wavelength of the two supermodes as discussed earlier. Fig. 4(b) shows the experimental results for electrostatically actuated PCNCs, illustrating the dependence of the even supermode eigenfrequencies on the applied bias voltage. It can be seen that 10 nm of tuning can be achieved using as little as 5 V of applied bias voltage. The inset shows the field profile of the even mode. It is important to emphasize that the Qs did not change significantly across the whole tuning range (data not shown) [42]. This is in stark contrast to tuning via free-carrier injection, which results in a significant reduction in the cavity Q due to free-carrier absorption [49]. It should also be noted that the devices were characterized using a free space resonant scattering technique [30], [46].

The aforementioned technique is advantageous for the realization of applications such as low-power optical switches and reconfigurable filters/routers. At this point, it is worth clarifying that the stiffness of the nanobeam is heavily dependent on its geometry. This means that by making the beams thinner or longer the sensitivity ($d\lambda/dV$) can be increased significantly. It is also important to emphasize that in the steady state, the system is not drawing any power from the bias source. This is of great practical interest for the realization of reconfigurable devices and systems. A drawback of this configuration is that the two beams can become permanently stuck together due to Van der Waals interactions if the applied voltage exceeds the pull-in voltage [50]. A simple solution for this would be to design devices with periodic projections to reduce the surface contact area. Another inherent limitation of this tuning method is the RC time constant (resistance $\times$ capacitance) of the parallel nanobeams. In our devices, simple calculations show that the resistance offered by the silicon nanobeams is on the order of $10^7\ \Omega$ (due to high resistivity of the SOI device layer: $1 - 10\,\Omega - $ cm), and the capacitance is on the order of 10^{-17} F, resulting in RC time constants in the nano-second range. Experimentally, however, we observed slower device response (on the order of a second) which can be attributed to parasitic capacitances (e.g., between large metal contacts and substrate) and resistances (e.g., due to lateral contact between metal and silicon). This response time could be readily improved by improving the conductivity of silicon by doping. Doping concentrations of 10^{18}cm^{-3} would reduce the resistivity by more than 2 orders of magnitude. The doping would also limit the Q values to the order of 10^5, which, however, is sufficient for most of the applications. More importantly, the performance of the system could be further improved by utilizing alternative actuation methods such as dielectrophoretic force [51] that do not depend on the RC time constant of the coupled nanobeams. In that case, the response time would be limited by the mechanical response, which is in present geometry on the order of 100 ns, and could be reduced to around 10 ns with modifications to geometry at the expense of the increased control voltage due to the increase stiffness of the structure.

B. All-Optical Reconfiguration Methods

Reconfiguration of PCNCs can also be achieved by using all-optical approaches. This scheme is not limited by external parasitic effects, does not require extra footprint for electrodes, and can be used to efficiently reconfigure multiple devices simultaneously. In our recent work [43], we demonstrated the use of optomechanical coupling to reconfigure waveguide coupled PCNCs. A high-power pump is used to generate an optical force to mechanical deform the nanobeams and detune the filter

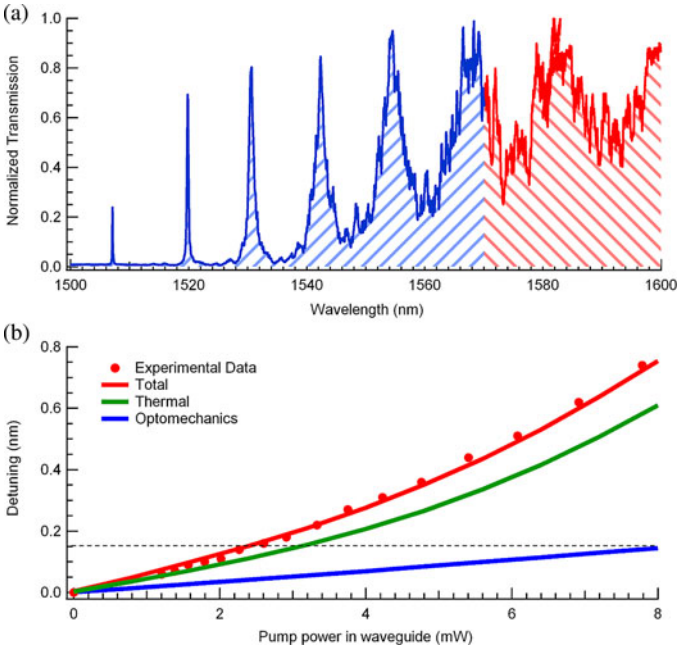

Fig. 5. Reconfigurable optomechanical optical filter. (a) Normalized transmission through suspended coupled PCNC structure. (b) Experimental data of detuning of filter mode for various pump powers. The red solid line is the fit and the green and blue solid lines are the extracted detuning contributions for thermal (due to optical excitation) and optomechanics, respectively.

mode. A low-power laser is used as a probe to scan around the filter resonance. Fig. 5(a) shows the transmission through the suspended coupled cavities. The device can be pumped at one of the higher order modes to take advantage of the optical Q to increase the stored energy inside the cavity. However, this configuration suffers from self-detuning of the pump mode resulting in reduction of stored optical energy or requirement of pump tracking. Hence, we pump the device outside the bandgap [red shaded area shown in Fig. 5(a)], using the allowed (propagating) modes of the photonic crystal. In future, this will also enable us to actuate the device using a broadband source as a pump, eliminating the requirement of a pump laser. Fig. 5(b) plots the experimental data showing the detuning of the filter mode for various pump powers. The red curve is the fit obtained using combined effects of thermal and optomechanical detuning [43], while their individual contributions are plotted in green (thermal due to material absorption) and blue (optomechanics). The dashed line denotes one linewidth detuning (150 pm) for a cavity with a Q of $10,000$. One can see that around 8 mW of optical power is sufficient to detune the cavity using an optomechanical approach only. This optical power can be generated using broadband LEDs and, hence, can be used to reconfigure multiple devices. At high input powers (large stored energy inside cavity), thermooptic effects arising from absorption due to free carriers generated by two-photon absorption contribute to the detuning as well [43].

It should be noted that the optical approach can also be used to thermally reconfigure the devices. As seen in [see Fig. 5(b)], nearly $80\,\%$ of the detuning in the all-optical case in silicon-based devices was due to heat [43]. However, such reconfiguration is limited in speed by the thermal decay rate that is much slower than mechanical reconfiguration rate, limited by the characteristic mechanical resonant frequency.

IV. Performance Comparison

To compare the tuning methods discussed previously, we consider three important performance characteristics (for filter and routing applications): hold power, maximum operating frequency, and tuning efficiency. Except for tuning efficiency, we compare reconfiguration based on one linewidth of detuning corresponding to a Q of $10,000$ (linewidth of 150 pm at operating wavelength of 1500 nm).

A. Hold Power

Tuning hold power is the power spent to hold the device in the reconfigured state. This property is an important figure of merit for postfabrication trimming and tuning techniques. The microheater-based thermal reconfiguration requires $250\,\mu$W of hold power as compared to negligible power consumption for the electromechanics case (due to the leakage current associated with the device). For optomechanics, we estimated the hold power to be 8 mW. This value is the optical power inside waveguide before the cavity. The hold power value for optomechanics can be lowered by reducing the widths of the waveguides or by increasing the suspended length (reducing the spring constant of the system). For example, if the width of the resonator is decreased by a factor of 2, the actuation power decreases by factor of 2 as well. Similarly, if the length of the waveguide is increased by a factor of 2, the actuation power decreases by factor of 8. However, this has an adverse effect on the operation speeds by reducing the fundamental resonance frequency of the device as discussed in the next section. The hold power can also be reduced by decreasing the gap between the suspended nanobeams, that is by increasing the amount of optomechanical coupling. For example, if the optomechanical coupling g_{om} defined as the change in resonant frequency for change in nanobeam separation gap, is increased by a factor of 2, the required detuning power reduces by a factor of 4. Finally, the hold power can be reduced by using high-Q modes that allow for build up of optical energy for even smaller powers in the waveguide. In the case of all optical thermo-optic technique, the hold power was found to be 3.1 mW.

B. Maximum Operating Frequency

Next, we compare the operational speeds for the three schemes. We note that the Q of the device under consideration is not high enough to limit the speed of operation. The speed of operation of thermal-based tuning method depends on the efficiency of heat transfer in the system. In order to estimate the thermal cutoff frequency, the maximum tuning frequency above which the device cannot respond to changes in temperature, we make use of the pump-probe scheme. Instead of coupled cavities, we use single suspended PCNC and sinusoidally modulate the high-power pump using an electro-optic modulator. Owing to thermal absorption of silicon, the portion of the pump

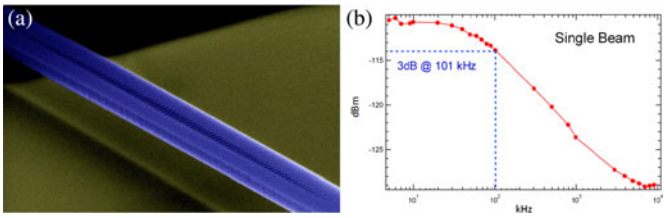

Fig. 6. Thermal response of PCNC. (a) SEM image of the single suspended PCNC used in the experiment. (b) Amplitude of the frequency response of the device. Thermal cutoff frequency is around 100 kHz.

power is absorbed by the suspended PCNC is converted into heat and the filter resonance is detuned due to thermo-optic effect. Furthermore, since the thermo-optic coefficient of silicon is positive, the filter mode resonance is shifted to longer wavelengths with increasing temperature. A low-power probe laser, positioned at the wavelength corresponding to the maximum slope of the filter mode (with pump off) is used to read out the transmitted intensity. The pump power is adjusted such that at low modulation frequencies (< 10 Hz) the filter resonance is detuned by a linewidth of the filter mode. The intensity of the transmitted probe laser is analyzed using an electrical spectrum analyzer (Tektronix RSA 3300) and the amplitude of the modulated probe signal is noted. The data obtained, which correspond to the amplitude of the frequency response of the device, is plotted in Fig. 6(b). The 3 dB point indicating the thermal cutoff frequency is found out to be 101 kHz. This sets a limit on the speed of operation of the device based on thermo-optic effects.

To compare our experimental results with theoretical predictions, we used FEM simulations. The thermal conductivity in thin and unpatterned SOI samples was measured by several groups, and it was found that the thermal conductivity strongly depends on the thickness of the sample [52]–[54]. For example, a thermal conductivity of $40\mathrm{W/mK}$ has been reported for 115-nm-thick silicon samples [52], ~ 4 times smaller than that of bulk silicon, while a thermal conductivity as low as $15\,\mathrm{W/mK}$ has been reported for polysilicon samples with 210 nm grains. We expect effective thermal conductivity in our devices to be comparable to that of the polycrystalline silicon, since the patterning (an array of holes) has similar characteristic length scale with mean hole-to-hole separation of 170 nm and the mean distance between the edge of the nanobeam and the holes 125 nm. Using FEM simulations, and fitting the data shown in Fig. 6(b), we were able to extract the value of thermal conductivity to be $20\,\mathrm{W/mK}$, which was ~ 8 times smaller than the bulk value.

The speed of electromechanical and optomechanical schemes is ultimately limited by the mechanical response of the structures. Electromechanics-based technique can be limited by *RC* time constants as seen earlier but this problem can be resolved by a proper design. The maximum speed of operation is set by the fundamental mechanical frequency, which in our case was around 10 MHz. Therefore, this reconfiguration scheme is suitable for signal routing and optical circuit switching applications. This mechanical frequency can be increased by increasing the stiffness of the beams but would in turn increase the energy required for reconfiguration [55].

C. Tuning Efficiency

Tuning efficiency can be defined as net detuning of the system per milliwatt of an applied power. Hence, it is the ratio between detuning and the power required to achieve the detuning. Tuning efficiency can be understood as a dynamical quantity (power required during reconfiguration) while hold power is its static counterpart that gives the steady-state power consumption. We found that electromechanics techniques has the maximum tuning efficiency of $8.9 \times 10^2\,\mathrm{nm/mW}$ (assuming zero contact resistance or parasitic capacitance) followed by electrical thermo-optic, all-optical thermo-optic, and optomechanic techniques at 0.625, 0.048, and $0.018\,\mathrm{nm/mW}$, respectively. For the all-optical case, it must be noted that the numbers are estimated using power inside the waveguide and not the actual power lost in the cavity during the reconfiguration process (which would be negligible). We also note that for all tuning methods, except for the electromechanics, tuning efficiency is inversely proportional to the hold power. In the case of electromechanics, power used to estimate the efficiency is actual power lost during the reconfiguration process (since steady-state hold power is zero). This explains significantly larger tuning efficiency for this method. The detuning expressions for the four reconfiguration techniques are as follows.

Electrical thermo-optic tuning efficiency is given by

$$\frac{\Delta\lambda}{P_{\mathrm{in}}} = \frac{\lambda_0 \Gamma^{\mathrm{th}} \frac{dn_{\mathrm{Si}}}{dT} \beta}{n_{\mathrm{Si}} C_{\mathrm{th}} \tau_{\mathrm{th}}}$$
$$\Gamma^{\mathrm{th}} = \frac{\int_{\mathrm{Si}} \epsilon(r) E^2(r) dv}{\int \epsilon(r) E^2(r) dv} \tag{2}$$

where $\Delta\lambda$ is the wavelength shift, dn_{Si}/dT is the thermo-optic coefficient of silicon, C_{th} the heat capacity, τth is the thermal decay rate, and β is the ratio of temperature of the nanobeam to the temperature of the heater.

Electromechanical tuning efficiency is given by

$$\frac{\Delta\lambda}{P_{\mathrm{cap}}} = 10 \cdot \frac{g_{\mathrm{om}} \cdot \tau_{\mathrm{cap}}}{d \cdot k} \tag{3}$$

where P_{cap} is the power needed to charge the capacitor (formed by two silicon nanobeams), d is the starting gap, k is the effective spring constant, τ_{cap} is the time constant of the system, and g_{om} is the optomechanical coupling constant of the filter defined as the change in resonant frequency for change in nanobeam separation gap.

Optomechanical tuning efficiency is given by

$$\frac{\Delta\lambda}{P_{\mathrm{in}}} = \frac{\lambda_0 g_{\mathrm{om}}^c g_{\mathrm{om}}^p 4 Q_t^2}{\omega_0^3 m_{\mathrm{eff}} \omega_p \Omega_m^2 Q_c} \tag{4}$$

where m_{eff} is the effective mass of the nanobeam, Ω_m is the frequency of the mechanical mode, $g_{\mathrm{om}}^{(c,p)}$ is the optomechanical coupling constant of the filter (pump) mode, and $Q_{\mathrm{abs}}, Q_{c,}$ and Q_t are the absorption, coupling, and total Qs, respectively. Note that the stored energy U is a nonlinear function of the input power at large powers due to optomechanics and material nonlinearities of silicon such as TPA, FCA, Kerr effect [43]. Broadband tuning using coupled ring resonators in silicon nitride has been demonstrated with efficiency of $2.5\,\mathrm{nm/mW}$. The

TABLE I
SUMMARY OF RECONFIGURATION TECHNIQUES

Technique	Hold Power	Maximum Operating Frequency	Tuning Efficiency
Thermo-optic (Electrical)	$250\ \mu W$ [a]	$> 100\ kHz$	$0.598\ nm/mW$
Electro-mechanic	negligible	$10\ MHz$ [b]	$8.9 \times 10^2\ nm/mW$ [d,e]
Opto-mechanic	$8\ mW$ [a,c,d]	$10\ MHz$ [b]	$0.018\ nm/mW$ [e]
Thermo-optic (All-optical)	$3.1\ mW$ [a,c]	$100\ kHz$ [b]	$0.048\ nm/mW$

[a] based on detuning one linewidth ($150\,\mathrm{pm}$) corresponding to a Q of $10,000$.
[b] limited by mechanics (10 MHz was the fundamental mechanical frequency of the device under test).
[c] optical power inside waveguide before cavity.
[d] estimated value in absence of contact resistance or parasitic capacitance.
[e] values increase for smaller gaps.

lower energy requirement comes from the fact that the scheme uses high-Q mode as a pump. However, unlike the previously described method of waveguide mode pumping, this scheme suffers from a pump mode detuning that requires a tunable laser source to track and follow the detuning of the pump mode and can be used to tune only one device at a time. We compared the numbers for PCNCs [43] using a high-Q (~ 5000) mode as a pump and the tuning efficiencies with and without tracking the pump for all-optical thermo-optic technique were 0.5 and $0.22\,\mathrm{nm/mW}$ while for optomechanic the values were 0.083 and $0.013\,\mathrm{nm/mW}$, respectively.

All optical thermo-optic tuning efficiency can be obtained from perturbation theory and is given by

$$\frac{\Delta\lambda}{P_{\mathrm{in}}} = \frac{\lambda_0 \Gamma^{\mathrm{th}} \frac{dn_{\mathrm{Si}}}{dT} 4Q_t^2}{n_{\mathrm{Si}} C_{\mathrm{th}} \tau_{\mathrm{th}} Q_{\mathrm{abs}} Q_c}. \tag{5}$$

V. SUMMARY, OUTLOOK, AND CONCLUSION

We have presented various techniques for reconfiguration of PCNCs. Table I compares the different techniques based on their tuning hold power, maximum operating frequency, and tuning efficiency. We found that, the electrical-based thermo-optic technique is the easiest to implement but is slow and requires an additional footprint for heater and contacts. The electromechanic-based technique is by far the most efficient technique and has higher operating speeds, though it also requires an additional footprint for the implementation of the electrical contacts. However, its negligible steady-state hold power makes it ideal for applications in a postfabrication trimming for realization of programmable optical circuits, optical circuit switching, and so on. All-optical based approaches overcome the additional footprint requirement but instead require nonzero steady-state hold powers.

One important reconfiguration methods not addressed in this study is based on free carrier injection. This methods can provide high speed of operation [56] but suffers from increased footprint requirement as any other electrical-based method. Thermal tuning can also be achieved by direct ohmic heating [57] in the device instead of using separate metal heaters as demonstrated earlier. Such technique showed a two fold improvement in the tuning efficiency in a ring resonator-based system. This technique can be implemented for PCNCs and would prove to be more efficient due to fewer carriers needed to be injected due to small mode volume of PCNC.

Here, we presented a compact optical resonators that can have performance on par to those found in ring resonators but in much smaller footprint: for a same Q, the Q/footprint ratio of a PCNC is higher than that of a ring resonator. For instance, the footprint requirement for a ring resonator with $2\ \mu$m radius is three times larger than that of a PCNC. Several research and industrial groups have proposed various architectural designs for multicore chips with integrated optical technologies. Most of the methods require an optical bus, in which waveguide crossings limit the device densities. A solution to this could be a multioptical plane architecture. PCNCs are well suited for this application as they can be designed to scatter light out of plane as shown earlier. Therefore, they can be used to efficiently communicate information between different planes. In network applications, multiple wavelengths (WDM) are required to be switched simultaneously. This can be effectively achieved using an optomechanical tuning approach for PCNCs: the same broadband pump can be used to reconfigure multiple devices, for example, in a filter bank. However, unlike ring resonators, PCNCs reflect most of the light and transmit only at resonant frequency. This reflected light can be detrimental for applications, and optical isolators or innovative designs may be needed [56], [58], [59]. It should be noted, however, that PCNCs can also be evanescently coupled and information can be read using a different input and output ports to improve the signal-to-noise-ratio [60].

In times to come, it will be clear to what extent photonic devices can replace electronic devices. Much will depend on the power requirements, speed of operation, robustness, long period drifts, system integration, and packaging of the devices. Photonic crystal nanobeam cavities have the potential to fulfill the aforementioned requirements and form a building block for achieving on-chip interconnect components for switching and signal routing applications. Their true potential and value for applications in data centers, however, will be in the end determined by the application specialists. We have seen that PCNCs are compatible with different reconfiguration techniques using thermo-optic, electromechanic, and optomechanic effects making them potential candidates for achieving reconfigurable photonic devices, especially for on-chip switching and routing applications. At the same time, PCNCs are indispensable for studies of light-matter interaction due to their ability to store photons in wavelength-scale volumes for many optical cycles, which makes them an interesting platform for sensing and cavity Quantum electrodynamics (QED) applications.

REFERENCES

[1] N. Magen, A. Kolodny, U. Weiser, and N. Shamir, "Interconnect-Power Dissipation in a Microprocessor," in *Proc. Int. Workshop Syst. Level Interconnect Prediction*, 2004, pp. 7–13.

[2] J. D. Meindl, J. A. Davis, P. Zarkesh-Ha, C. S. Patel, K. P. Martin, and P. A. Kohl, "Interconnect opportunities for gigascale integration," *IBM J. Res. Devel.*, vol. 46, pp. 245–263, 2002.

[3] R. Ho, K. Mai, and M. Horowitz, "The future of wires," *Proc. IEEE*, vol. 89, no. 4, pp. 490–504, Apr. 2001.

[4] A. F. Benner, M. Ignatowski, J. A. Kash, D. M. Kuchta, and M. B. Ritter, "Exploitation of optical interconnects in future server architectures," *IBM J. Res. Devel.*, vol. 49, pp. 755–775, 2005.

[5] D. Miller, "Device requirements for optical interconnects to silicon chips," *Proc. IEEE*, vol. 97, no. 7, pp. 1166–1185, Jul. 2009.

[6] D. A. B. Miller, "Rationale and challenges for optical interconnects to electronic chips," *Proc. IEEE*, vol. 88, no. 6, pp. 728–749, Jun. 2000.

[7] C. Hermans and M. Steyaert, *Broadband Opto-Electrical Receivers in Standard CMOS*. New York: Springer-Verlag, 2007.

[8] T. Koonen, "Fiber to the home/fiber to the premises: What, where, and when?" *Proc. IEEE*, vol. 94, no. 5, pp. 911–934, May 2006.

[9] R. Beausoleil, P. Kuekes, G. Snider, S.-Y. Wang, and R. Williams, "Nanoelectronic and nanophotonic interconnect," *Proc. IEEE*, vol. 96, no. 2, pp. 230–247, Feb. 2008.

[10] A. Shacham, K. Bergman, and L. Carloni, "Photonic networks-on-chip for future generations of chip multiprocessors," *IEEE Trans. Comput.*, vol. 57, no. 9, pp. 1246–1260, Sep. 2008.

[11] W. M. Green, M. J. Rooks, L. Sekaric, and Y. A. Vlasov, "Ultra-compact, low RF power, 10 GB/s silicon Mach-Zehnder modulator," *Opt. Expr.*, vol. 15, no. 25, pp. 17106–17113, 2007.

[12] V. R. Almeida, C. A. Barrios, R. R. Panepucci, and M. Lipson, "All-optical control of light on a silicon chip," *Nature*, vol. 431, pp. 1081–1084, 2004.

[13] M. A. Popovíc, T. Barwicz, M. R. Watts, P. T. Rakich, L. Socci, E. P. Ippen, and F. X. Kärtner, H. I. Smith, "Multistage high-order microring-resonator add-drop filters," *Opt. Lett.*, vol. 31, no. 17, pp. 2571–2573, 2006.

[14] F. Xia, M. Rooks, L. Sekaric, and Y. Vlasov, "Ultra-compact high order ring resonator filters using submicron silicon photonic wires for on-chip optical interconnects," *Opt. Expr.*, vol. 15, no. 19, pp. 11934–11941, 2007.

[15] J. Pan, Y. Huo, K. Yamanaka, S. Sandhu, L. Scaccabarozzi, R. Timp, M. L. Povinelli, S. Fan, M. M. Fejer, and J. S. Harris, "Aligning microcavity resonances in silicon photonic-crystal slabs using laser-pumped thermal tuning," *Appl. Phys. Lett.*, vol. 92, pp. 103–114, 2008.

[16] I. Märki, M. Salt, H. P. Herzig, R. Stanley, L. E. Melhaoui, P. Lyan, and J. M. Fedeli, "Optically tunable microcavity in a planar photonic crystal silicon waveguide buried in oxide," *Opt. Lett.*, vol. 31, no. 4, pp. 513–515, 2006.

[17] F. Ilya, W. Edo, E. Dirk, S. Nick, P. Pierre, and V. Jelena, "Ultrafast nonlinear optical tuning of photonic crystal cavities," *Appl. Phys. Lett.*, vol. 90, no. 9, pp. 091118–091118-3, 2007.

[18] M. W. McCutcheon, A. G. Pattantyus-Abraham, G. W. Rieger, and J. F. Young, "Emission spectrum of electromagnetic energy stored in a dynamically perturbed optical microcavity," *Opt. Expr.*, vol. 15, no. 18, pp. 11472–11480, 2007.

[19] M. Eichenfield, R. Camacho, J. Chan, K. J. Vahala, and O. Painter, "A picogram- and nanometre-scale photonic-crystal optomechanical cavity," *Nature*, vol. 459, no. 7246, pp. 550–555, 2009.

[20] M. Li, W. H. P. Pernice, and H. X. Tang, "Tunable bipolar optical interactions between guided lightwaves," *Nature Photon.*, vol. 3, no. 8, pp. 464–468, 2009.

[21] G. Wiederhecker, L. Chen, A. Gondarenko, and M. Lipson, "Controlling photonic structures using optical forces," *Nature*, vol. 462, no. 7273, pp. 633–636, 2009.

[22] S. J. McNab, N. Moll, and Y. A. Vlasov, "Ultra-low loss photonic integrated circuit with membrane-type photonic crystal waveguides," *Opt. Expr.*, vol. 11, pp. 2927–2939, 2003.

[23] Q. M. Quan, P. B. Deotare, and M. Loncar, "Photonic crystal nanobeam cavity strongly coupled to the feeding waveguide," *Appl. Phys. Lett.*, vol. 96, no. 20, pp. 203102–203102-3, 2010.

[24] Q. M. Quan and M. Loncar, "Deterministic design of wavelength scale, ultra-high q photonic crystal nanobeam cavities," *Opt. Expr.*, vol. 19, no. 19, pp. 18529–18542, 2011.

[25] T. Barwicz, M. A. Popovic, P. T. Rakich, M. R. Watts, H. A. Haus, E. P. Ippen, and H. I. Smith, "Microring-resonator-based add-drop filters in SiN: Fabrication and analysis," *Opt. Expr.*, vol. 12, no. 7, pp. 1437–1442, 2004.

[26] B. B. C. Kyotoku, L. Chen, and M. Lipson, "Sub-nm resolution cavity enhanced microspectrometer," *Opt. Expr.*, vol. 18, no. 1, pp. 102–107, 2010.

[27] Z. Xia, A. A. Eftekhar, M. Soltani, B. Momeni, Q. Li, M. Chamanzar, S. Yegnanarayanan, and A. Adibi, "High resolution on-chip spectroscopy based on miniaturized microdonut resonators," *Opt. Expr.*, vol. 19, no. 13, pp. 12356–12364, 2011.

[28] C. Sauvan, G. Lecamp, P. Lalanne, and J. P. Hugonin, "Modal-reflectivity enhancement by geometry tuning in photonic crystal microcavities," *Opt. Expr.*, vol. 13, no. 1, pp. 245–255, 2005.

[29] A. R. M. Zain, N. P. Johnson, M. Sorel, and R. M. De la Rue, "Ultra high quality factor one dimensional photonic crystal/photonic wire micro-cavities in silicon-on-insulator (SOI)," *Opt. Expr.*, vol. 16, no. 16, pp. 12084–12089, 2008.

[30] P. B. Deotare, M. W. McCutcheon, I. W. Frank, M. Khan, and M. Loncar, "High quality factor photonic crystal nanobeam cavities," *Appl. Phys. Lett.*, vol. 94, no. 12, pp. 121106–121106-3, 2009.

[31] L. Chen, N. Sherwood-Droz, and M. Lipson, "Compact bandwidth-tunable microring resonators," *Opt. Lett.*, vol. 32, no. 22, pp. 3361–3363, 2007.

[32] A. H. Atabaki, E. S. Hosseini, A. A. Eftekhar, S. Yegnanarayanan, and A. Adibi, "Optimization of metallic microheaters for high-speed reconfigurable silicon photonics," *Opt. Expr.*, vol. 18, no. 17, pp. 18312–18323, 2010.

[33] T. Fukazawa, F. Ohno, and T. Baba, "Very compact arrayed-waveguide-grating demultiplexer using Si photonic wire waveguides," *Jpn. J. Appl. Phys.*, vol. 43, pp. L673–L675, 2004.

[34] J. Brouckaert, W. Boagerts, S. Selvaraja, P. Dumon, R. Baets, and D. Van Thourhout, "Planar concave grating demultiplexer with high reflective bragg reflector facets," *IEEE Photon. Technol. Lett.*, vol. 20, no. 4, pp. 309–311, Feb. 2008.

[35] B. Momeni, E. S. Hosseini, M. Askari, M. Soltani, and A. Adibi, "Integrated photonic crystal spectrometers for sensing applications," *Opt. Commun.*, vol. 282, no. 15, pp. 3168–3171, 2009.

[36] F. Horst, W. M. J. William, B. J. Offrein, and Y. A. Vlasov, "Silicon-on-insulator echelle grating WDM demultiplexers with two stigmatic points," *IEEE Photon. Technol. Lett.*, vol. 21, no. 23, pp. 1743–1745, Dec. 2009.

[37] J. Song and N. Zhu, "Design and fabrication of compact etched diffraction grating demultiplexers based on-Si nanowire technology," *Electron. Lett.*, vol. 44, no. 13, pp. 816–818, 2008.

[38] F. Horst, M. J. G. William, B. J. Offrein, and Y. A. Vlasov, "Echelle grating WDM (de-)multiplexers in SOI technology, based on a design with two Stigmatic points," in *Proc. SPIE Silicon Photon. Photon. Integrated Circuits*, 2008, vol. 6996, pp. 69960R–69960R-8.

[39] L. Chen and M. Lipson, "Ultra-low capacitance and high speed germanium photodetectors on silicon," *Opt. Expr.*, vol. 17, no. 10, pp. 7901–7906, 2009.

[40] S. Noda, A. Chutinan, and M. Imada, "Trapping and emission of photons by a single defect in a photonic bandgap structure," *Nature*, vol. 407, pp. 608–610, 2000.

[41] M. Li, W. Pernice, C. Xiong, M. Baehr-Jones, Tand Hochberg, and H. Tang, "Harnessing optical forces in integrated photonic circuits," *Nature*, vol. 456, no. 7221, pp. 480–484, 2008.

[42] P. B. Deotare, M. W. McCutcheon, I. W. Frank, M. Khan, and M. Lončar, "Coupled photonic crystal nanobeam cavities," *Appl. Phys. Lett.*, vol. 95, no. 3, pp. 031102–031102-3, 2009.

[43] P. B. Deotare, I. Bulu, I. W. Frank, Q. Quan, Y. Zhang, R. Ilic, and M. Loncar, "All optical reconfiguration of optomechanical filters," *Nature Commun.*, vol. 3, no. 846, pp. 846–846-8, 2012.

[44] M. A. Popovic, C. Manolatou, and M. R. Watts, "Coupling-induced resonance frequency shifts in coupled," *Opt. Expr.*, vol. 14, no. 3, pp. 1208–1222, 2006.

[45] S. G. Johnson, M. Ibanescu, M. A. Skorobogatiy, O. Weisberg, J. D. Joannopoulos, and Y. Fink, "Perturbation theory for Maxwell's equations with shifting material boundaries," *Phys. Rev. E*, vol. 65, pp. 066611–066611-7, 2002.

[46] I. W. Frank, P. B. Deotare, M. W. McCutcheon, and M. Loncar, "Programmable photonic crystal nanobeam cavities," *Opt. Expr.*, vol. 18, no. 8, pp. 8705–8712, 2010.

[47] X. Y. Chew, G. Y. Zhou, F. S. Chau, J. Deng, X. S. Tang, and Y. C. Loke, "Dynamic tuning of an optical resonator through mems-driven coupled photonic crystal nanocavities," *Opt. Lett.*, vol. 35, no. 15, pp. 2517–2519, 2010.

[48] R. Perahia, J. D. Cohen, S. Meenehan, T. P. M. Alegre, and O. Painter, "Electrostatically tunable optomechanical 'zipper' cavity laser," *Appl. Phys. Lett.*, vol. 97, no. 19, pp. 191112–191112-3, 2010.
[49] K. Djordjev, S.-J. Choi, S.-J. Choi, and P. D. Dapkus, "Microdisk tunable resonant filters and switches," *IEEE Photon. Technol. Lett.*, vol. 14, no. 6, pp. 828–830, Jun. 2002.
[50] C. Liu, *Foundations of MEMS*. Englewood Cliffs, NJ: Prentice Hall, 2005.
[51] Q. P. Unterreithmeier, E. M. Weig, and J. P. Kotthaus, "Universal transduction scheme for nanomechanical systems based on dielectric forces," *Nature*, vol. 458, no. 7241, pp. 1001–1004, 2009.
[52] A. K. E. G. McConnell, "Thermal conduction in silicon micro and nanostructures," *Annu. Rev. Heat Transf.*, vol. 14, pp. 129–168, 2005.
[53] W. J. Liu and M. Asheghi, "Thermal conduction in ultrathin pure and doped single-crystal silicon layers at high temperatures," *J. Appl. Phys.*, vol. 98, pp. 123523–123523-6, 2005.
[54] W. Liu and M. Asheghi, "Thermal conductivity measurements of ultrathin single crystal silicon layers," *J. Heat Transf.—Trans. ASME*, vol. 128, no. 1, pp. 75–83, 2006.
[55] Y. T. Yang, K. L. Ekinci, X. M. H. Huang, L. M. Schiavone, M. L. Roukesa, C. A. Zorman, and M. Mehregany, "Monocrystalline silicon carbide nanoelectromechanical systems," *Appl. Phys. Lett.*, vol. 78, no. 2, pp. 162–164, 2001.
[56] Q. Xu, S. Manipatruni, B. Schmidt, J. Shakya, and M. Lipson, "12.5 Gbit/s carrier-injection-based silicon micro-ring silicon modulators," *Opt. Expr.*, vol. 15, no. 2, pp. 430–436, 2007.
[57] S. Manipatruni, R. K. Dokania, B. Schmidt, N. Sherwood-Droz, C. B. Poitras, A. B. Apsel, and M. Lipson, "Wide temperature range operation of micrometer-scale silicon electro-optic modulators," *Opt. Lett.*, vol. 33, no. 19, pp. 2185–2187, 2012.
[58] S. Fan, P. R. Villeneuve, J. D. Joannopoulos, and H. A. Haus, "Channel drop filters in photonic crystals," *Opt. Expr.*, vol. 3, no. 1, pp. 4–11, 1998.
[59] Z. Yu and S. Fan, "Complete optical isolation created by indirect interband photonic transitions," *Nature Photon.*, vol. 3, pp. 91–94, 2009.
[60] B. Cluzel, K. Foubert, L. Lalouat, J. Dellinger, D. Peyrade, E. Picard, E. Hadji, and F. Fornel1, "Addressable subwavelength grids of confined light in a multislotted nanoresonator," *Appl. Phys. Lett.*, vol. 98, no. 8, pp. 081101–081101-3, 2011.

Parag B. Deotare (S'11) received the B.E. and M.S. degrees from the University of Pune, India, and Texas A&M University, in electrical engineering in 2004 and 2007, respectively, and the Ph.D. degree from Harvard University, Cambridge, MA, in 2012.

He is currently a Postdoctoral Associate in Organic and Nanostructured Electronics Laboratory, Massachusetts Institute of Technology, Cambridge. His current research interests include reconfigurable photonics, optomechanics, and light matter interaction between optical nanocavities and organic materials.

Leonard C. Kogos received the B.S. degree in electrical engineering and computer science from Harvard University, Cambridge, MA, in 2012.

He is currently a Research Associate in Schlumberger Doll-Research Center, Cambridge, MA. His research interests include silicon photonics, spectroscopy, on chip sensing, and NMR sensing.

Irfan Bulu received the Ph.D. degree in 2007, from Bilkent University, Ankara, Turkey.

He is currently a Research Scientist in Harvard University, Cambridge, MA, in applied physics. His research interests include on-chip optical spectroscopy techniques, nonlinear photonic devices for all optical information processing at the classical and quantum level, development of novel light sources, and cavity optomechanics.

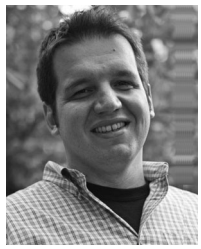

Marko Lončar (SM'12) received the Diploma in 1997 from the University of Belgrade, Belgrade, Serbia, and the M.S. and Ph.D. degrees in 1998 and 2003, respectively, from the California Institute of Technology, Pasadena, all in electrical engineering.

He is a Tiantsai Lin Professor of electrical engineering in Harvard School of Engineering and Applied Sciences, Cambridge, MA. His recent research interests include optical nanocavities, diamond nanophotonics and quantum optics, nanoscale optomechanics, and cavity-based bio-chemical sensing. He is a recipient of the US National Science Foundation CAREER Award in 2009, and the Alfred P. Sloan Fellowship in 2010.